Analysis of carrier transport and band tail states in *p*-type tin monoxide thin-film transistors by temperature dependent characteristics

Jiawei Zhang,[1,a)] Xi Kong,[2,a)] Jia Yang,[2] Yunpeng Li,[2] Joshua Wilson,[1] Jie Liu,[3] Qian Xin,[2,b)] Qingpu Wang,[2] and Aimin Song[1,b)]
[1]*School of Electrical and Electronic Engineering, University of Manchester, Manchester M13 9PL, United Kingdom*
[2]*School of Physics, Shandong University, Jinan 250100, People's Republic of China*
[3]*State Key Laboratory of Crystal Materials, Shandong University, Jinan, 250100, People's Republic of China*

(Received 13 October 2015; accepted 14 June 2016; published online 30 June 2016)

Tin monoxide (SnO) has drawn much attention in recent years due to its high hole mobility, transparency, and potential for mass production. However, due to its metastable nature, the deposited film often contains multi-phases such as metallic tin and tin dioxide, which may degrade its electrical properties. Here, we presented the temperature dependent characteristics of *p*-type SnO thin-film transistors. The hole transport mechanism is dominated by band conduction at high temperatures and variable-range hopping at low temperatures. The maximum activation energy was found to be 308 meV, which denotes a bandgap of around 0.6 eV. The density of states was found to be $1.12 \times 10^{21}\,cm^{-3}\,eV^{-1}$ at $V_G = -80$ V, and $6.75 \times 10^{20}\,cm^{-3}\,eV^{-1}$ at $V_G = 0$ V, respectively. *Published by AIP Publishing*. [http://dx.doi.org/10.1063/1.4955124]

Metal oxide semiconductors such as indium-gallium-zinc-oxide (IGZO) have already started to be used in industry, in particular, to replace amorphous silicon for high-end display drivers.[1–3] However, most metal oxide semiconductors are *n*-type.[1–3] In order to develop complementary circuits by using metal oxides, it is necessary to find *p*-type oxide semiconductors.[2] However, it is difficult to obtain a *p*-type oxide with a high hole mobility since O 2p orbitals are likely to form the localized valence band maximum (VBM) which causes percolation and hopping conduction.[2,4] In recent years, tin monoxide (SnO) was found to be a promising *p*-type oxide as its VBM was composed of hybridized orbitals of Sn 5s and O 2p.[2,4–9] This valance band structure gives SnO the potential to obtain a hole mobility higher than $10\,cm^2\ V^{-1}\ s^{-1}$.[8] However, unlike another tin oxidation state, tin dioxide (SnO_2), SnO is a metastable phase and sensitive to temperature.[1] Thus, physical vapour deposition requiring high temperature processes becomes challenging for SnO. The most common method of SnO deposition is reactive radio-frequency (RF) sputtering using a metallic Sn target followed by a low-temperature thermal annealing process.[6,9–11] The *p*-type SnO can only be obtained in a narrow window of growth conditions.[8] It is found that the obtained film often shows multi-phases including metallic tin (Sn) and SnO_2, rather than pure SnO.[2] Many studies have shown that the on/off ratios of SnO thin-film transistors (TFTs) are around 10^3 at room temperature (RT),[2,4,8,9] which is much lower than the values obtained from IGZO TFTs.[12] Such high off current may be attributed to defects in the bandgap and the carrier transport mechanism in the VBM.[4] However, for such a disordered system, the carrier transport mechanism remains debatable.[13] Percolation conduction, where the carrier paths circumvent the high potential barriers above the mobility edge, has been regarded as a plausible carrier transport mechanism in disordered systems.[14] For amorphous IGZO, it is found that the log of conductivity (σ) follows a $T^{-1/4}$ law at low temperatures, suggesting a carrier transport regime dominated by percolation conduction.[15] However, another explanation for the $T^{-1/4}$ behaviour is Mott's variable-range hopping (VRH), which suggests that a carrier hops between localized sites.[16] VRH has been widely observed in non-crystalline materials, highly doped crystalline semiconductors, and polycrystalline semiconductors.[13,16,17] Trap-limited conduction model has also been raised to describe the carrier transport in amorphous semiconductors when the tail state energy is higher than the thermal energy at low temperature where log (σ) is proportional to T^{-1}.[18] At higher temperatures, where the carriers have the energies higher than the mobility edge, band conduction dominates the carrier transport, and log(σ) follows a T^{-1} law.[15]

The temperature dependent mobility and carrier concentration of SnO films obtained by Hall effect measurements have been discussed in several studies, which found that both mobility and carrier concentration exhibited thermally activated behaviours.[2,6] The temperature dependent hole concentration can be explained by the existence of a shallow acceptor level, but the reason for the thermally activated mobility remains unclear. However, compared with the Hall effect measurements, the characteristics of the thin-film transistors at different temperatures are able to reveal more properties within the bandgap.[13] The Fermi level (E_F) at the interface can be modified by changing the gate voltage (V_G). However, so far, the characteristics of SnO TFTs have only been studied from 298 K to 348 K, where the band conduction dominates.[19] By analyzing the temperature dependent characteristics of the TFT in off state at lower temperatures, the reasons for the high off current can be elucidated.

In this letter, we present the temperature dependent characteristics of the SnO TFT. The carrier transport

[a)]J. Zhang and X. Kong contributed equally to this work.
[b)]Authors to whom correspondence should be addressed. Electronic addresses: xinq@sdu.edu.cn and A.Song@manchester.ac.uk.

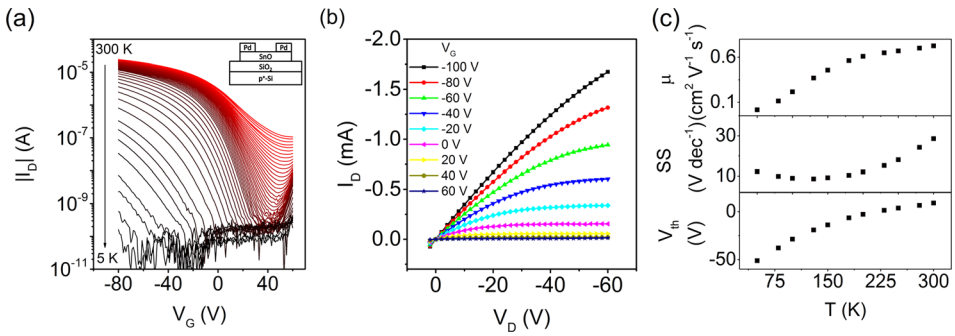

FIG. 1. (a) Transfer characteristics of the SnO TFT at temperatures from 300 K to 5 K. The inset shows the cross-section of the TFT. (b) Output characteristics of the SnO TFT at RT. (c) Mobility, subthreshold swing, and threshold voltage of the SnO TFT at different temperatures.

mechanisms at different temperatures are discussed. The activation energy, E_a, at different gate voltages is obtained. We also demonstrate and evaluate the density of states, $N(E)$, in the bandgap of the SnO film.

Bottom gate top contact TFTs were fabricated on thermally oxidized SiO_2/p^+-Si substrates. The thickness of the SiO_2 layer was 300 nm. Patterns were defined by shadow masks. A 27 nm-thick SnO film was deposited by reactive RF sputtering by using a Sn target with a substrate temperature of 100 °C. The argon/oxygen ratio was 23:3 during the deposition. The deposition power was fixed at 150 W, and the pressure was 4.3 mTorr. Before forming the source and drain, the SnO film was annealed in air at 225 °C for 1 h. The source and drain were formed by 50 nm-thick Pd contacts which were deposited by using an electron-beam evaporator. The channel width, W, is 2000 μm and the channel length, L, is 60 μm. The current-voltage characteristics were measured using Agilent B2902A source/measure unit at room temperature (RT) in dark. The low temperature measurements were performed with a 4 K helium cryostat from 5 K to 300 K in vacuum. The sample for the X-ray diffraction (XRD) analysis was prepared on a Si-SiO_2 wafer under the same deposition conditions. The XRD image of the 1 μm-thick SnO film was obtained using a D8 Advance X-ray diffractometer.

The transfer characteristics of the SnO TFT measured in vacuum from 300 K to 5 K are shown in Fig. 1(a). The drain voltage, V_D, was set to −1 V. The output characteristics of the SnO TFT at RT are shown in Fig. 1(b), which suggests that the TFT is in the linear regime when $V_D = -1$ V. In the transfer curve, the drain current, I_D, drops with the temperature. At RT, the off current is around 10^{-7} A, which is quite high compared with the gate leakage current (around 10^{-10} A). At temperatures around 150 K, the off current drops to 10^{-10} A and becomes dominated by the leakage current. By using $I_D = \mu C_{ox} \frac{W}{L} \left[(V_G - V_{th})V_D - \frac{1}{2}V_D^2\right]$, where C_{ox} is the dielectric capacitance per unit area and V_{th} is the threshold voltage, the mobility, μ, is found to be 0.73 $cm^2\ V^{-1}\ s^{-1}$ at RT and it decreases with the temperature as shown in Fig. 1(c). The threshold voltage decreases when decreasing the temperature. The subthreshold swing (SS) decreases beyond 150 K and reaches a minimum around 100 K. When the temperature is lower than 100 K, SS starts to increase with decreasing temperature. The lowest SS is found to be 8.6 V dec^{-1} at 130 K which corresponds to a total interface trap density of $1.02 \times 10^{13}\ cm^{-2} eV^{-1}$. In Figs. 2(a) and 2(b), the output characteristics of the SnO TFT at 200 K are shown from 0 V to 50 V and 80 V to 100 V.

Figure 3(a) shows the drain current at different temperatures from 300 K to 10 K with various gate voltages. At high temperatures, $\ln(I_D)$ is found to be proportional to T^{-1}. According to the band conduction model, the results follow the Arrhenius equation[20,21]

$$I_D = I_{D0} \exp(-E_a/k_B T), \tag{1}$$

where k_B is the Boltzmann constant, E_a is the activation energy, and I_{D0} is a prefactor of I_D. For n-type conduction, E_a equals $(E_C\text{-}E_F)$, and for p-type conduction, E_a equals $(E_F\text{-}E_V)$.[22] Thus, the activation energy can be obtained. Fig. 3(b) shows the relationship between E_a and V_G. In the linear region, the minimum E_a is around 14 meV. With the increasing gate voltage, the activation energy E_a also increases until reaching a maximum at around 0.3 eV. However, above 40 V, E_a starts to decrease, suggesting that the Fermi level becomes closer to the conduction band. As shown in Fig. 1(a), the drain current increases with the gate

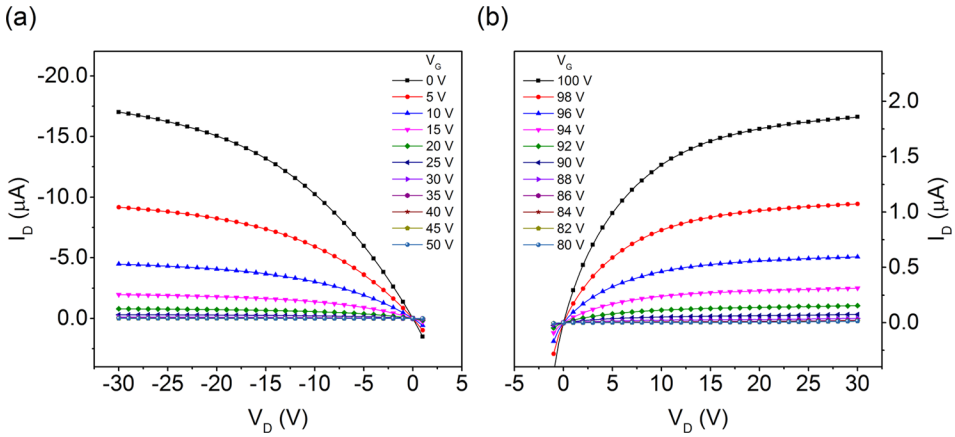

FIG. 2. Output characteristics of the SnO TFT at 200 K with gate voltages (a) from 0 V to 50 V, and (b) from 80 V to 100 V.

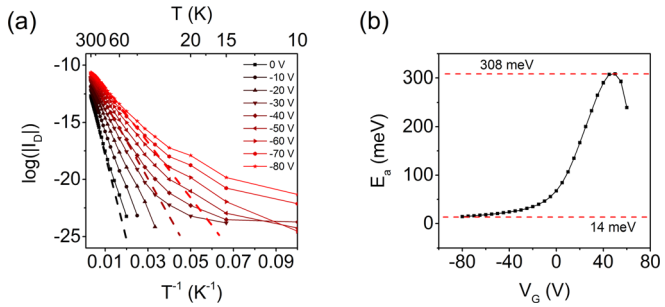

FIG. 3. (a) Drain current as a function of T^{-1} with gate voltages from 0 V to −80 V. Dashed lines indicate that the curves loses linearity at low temperatures. (b) Extracted activation energy at different gate voltages.

voltage beyond around 40 V at low temperatures, indicating *n*-type field-effect behaviour. This agrees well with the output characteristics at 200 K shown in Figs. 2(a) and 2(b). Similar observations of ambipolar behaviour have also been observed in Refs. 11 and 23. Hence, the SnO film starts to accumulate electrons to form an *n*-type channel, indicating that the bandgap of SnO is around 0.6 eV, which agrees well with the theoretical indirect bandgap of SnO.[2,6,23] The gradual increase in E_a may be attributed to the trap states in the SnO film.[24] When the temperature is lower than 80 K, as shown in Fig. 3(a), the $\ln(I_D) - T^{-1}$ curves become nonlinear, which suggests that the Arrhenius equation cannot be used to describe the drain current. This indicates that at low temperatures, band conduction is no longer the dominant transport mechanism in the SnO film.

However, Fig. 4(a) shows that $\ln(I_D)$ becomes linearly dependent on $T^{-1/4}$ at temperatures lower than 80 K. According to the percolation theory, the mobility is more likely to increase with the carrier concentration as the paths of the electrons with higher energies are shorter.[12] Since the hole mobility of SnO films has no clear dependencies on the hole carrier concentrations,[8] carrier transport is more likely to occur through variable-range hopping rather than percolation conduction. Thus, according to Mott's equation, the relationship between I_D and T is given by

$$I_D = I_{D0} \exp\left\{-2\left[\frac{\alpha^3}{k_B N(E) T}\right]^{\frac{1}{4}}\right\}, \tag{2}$$

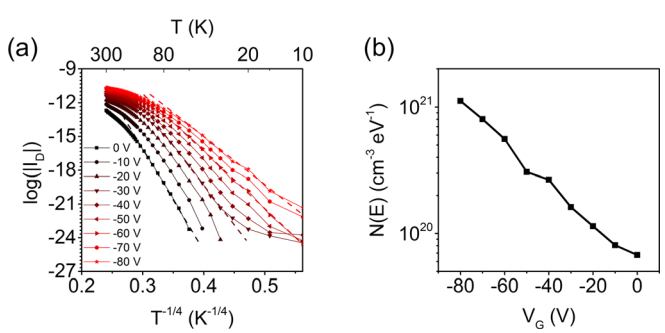

FIG. 4. (a) Drain current as a function of $T^{-1/4}$ with gate voltages from 0 V to −80 V. The linear fittings are shown as dashed lines. (b) Density of states obtained from Mott's equation as a function of gate bias.

where $N(E)$ is the density of states at the Fermi level and α is the reciprocal of the Bohr radius, a. For SnO, $a = a_0 \varepsilon_r m_0/m^*$, where a_0 is the Bohr radius of a hydrogen atom, 0.53 Å, ε_r is the permittivity of SnO which is 15, m_0 is the free electron mass, and m^* is the effective mass of holes in the valance band in SnO which is around $2.05m_0$.[4] Thus, the Bohr radius of SnO is calculated to be 3.87 Å. Mott's VRH model indicates that the access current in the Arrhenius plot is caused by carriers tunnelling between localized states close to the Fermi level.

According to Eq. (2), the density of states of SnO can be expressed as a function of I_D. In Fig. 4(b), a plot of $N(E)$ as a function of V_G was obtained. The density of states at the Fermi level is found to be $1.12 \times 10^{21}\,\mathrm{cm^{-3}\,eV^{-1}}$ at $V_G = -80$ V, and $6.75 \times 10^{20}\,\mathrm{cm^{-3}\,eV^{-1}}$ at $V_G = 0$ V, respectively. According to the VRH model, a carrier hops between the adjacent localized states. The most probable hopping distance and the average hopping energy are given by

$$R_{hop} = \left(\frac{3}{2\pi\alpha N(E) k_B T}\right)^{1/4}, \tag{3}$$

and

$$W_{hop} = \frac{3}{4\pi N(E) R_{hop}^3}. \tag{4}$$

Using the value of $N(E)$ determined previously, R_{hop} and W_{hop} were calculated and shown in Fig. 5(a). As expected, when decreasing the temperature, the most probable hopping distance increases and the average hopping energy decreases. As shown in Fig. 3(b), the density of states at $V_G = -80$ V is higher than the value at $V_G = 0$ V. As a result, at $V_G = -80$ V, the hopping distance becomes shorter and the average hopping energy is lower.

In crystalline SnO, the defects are mainly composed of tin vacancies (V_{Sn}), oxygen vacancies (V_O), interstitial tin atoms (Sn_i), and interstitial oxygen atoms (O_i).[25] According to first principle calculations, the *p*-type conductivity of SnO is caused by V_{Sn}.[25] V_{Sn} contributes to acceptor-like shallow defect states which may correspond to the density of states shown in Fig. 4(b). The inhomogeneities at the VBM may also contribute to the large density of states. The oxygen vacancies may distort the potentials of neighbouring atoms and cause shallow defect states near the VBM and CBM.

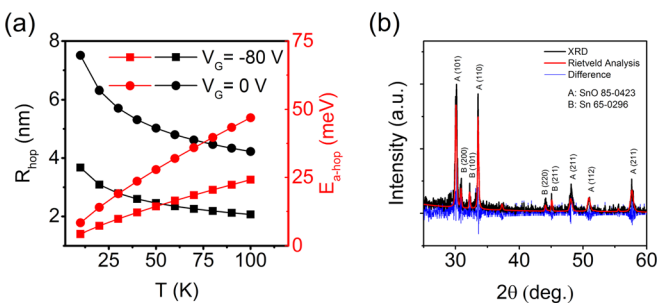

FIG. 5. (a) Most probable hopping distance and the average hopping energy as a function of temperature at $V_G = 0$ V and $V_G = -80$ V. (b) XRD image of the SnO film, which shows the presence of Sn (PDF 65-0296) and SnO (PDF 85-0423).

However, at RT, the concentration of V_O is orders of magnitude smaller than the concentration of V_{Sn}, which means it is unlikely that V_O will affect the *p*-type conductivity.[25] The interstitial oxygen atoms are likely to become O^{2-} and ionize Sn^{2+} to Sn^{4+} to maintain charge neutrality, which may improve electron transport in the CBM. Tin interstitial atoms create huge defect states between the planes of the SnO crystal, where hole transport predominantly occurs.[25] Thus, both tin and oxygen interstitials may contribute to the observed large *N(E)*.

In Fig. 5(b), the XRD image of a 1 μm-thick SnO film shows that there are excess Sn atoms (mass fraction of 12.75% according to the Rietveld analysis) remaining after annealing the sample at 225 °C for 1 h. As the *p*-type conductivity implies the existence of tin vacancies,[25] it suggests that there are excess O atoms in the SnO film. The redundant Sn and O atoms may originate from incomplete reactions during the deposition and thermal annealing of the SnO film. It is plausible that the interstitial Sn and O atoms could cause large defect states in the bandgap and thus result in a high off current at RT. As those defects are mainly composed of the Sn 5p-orbitals and O 2p-orbitals,[25] at low temperatures, hopping between localized states becomes more difficult, resulting in a lower off current.

For SnO TFTs, two types of hole transport mechanisms have been observed at different temperatures. The analysis of band conduction revealed that the maximum activation energy was around 0.3 eV and the bandgap was around 0.6 eV, which agrees well with the theoretical value. Carrier transport at low temperatures (<80 K) was dominated by VRH. In the $\ln(I_D) - T^{-1}$ regime, the role of the tail states could be further evaluated by the trap-limited conduction theory.[18] A large trap density of states was also observed in the VRH regime, which may be attributed to the interstitial Sn and O atoms present in the film.

We are grateful to the support from North-West Nanoscience Doctoral Training Centre, EPSRC Grant No. EP/G03737X/1. This work was financed by the National Natural Science Foundation of China (Grant Nos. 11374185 and 11304180), the Natural Science Foundation of Shandong Province (ZR2013EMQ011), and an Independent Innovation Fund of Shandong University (2013TB008).

[1]E. Fortunato, P. Barquinha, and R. Martins, Adv. Mater. **24**(22), 2945 (2012).
[2]Y. Ogo, H. Hiramatsu, K. Nomura, H. Yanagi, T. Kamiya, M. Hirano, and H. Hosono, Appl. Phys. Lett. **93**(3), 032113 (2008).
[3]J.-S. Park, H. Kim, and I.-D. Kim, J. Electroceram. **32**(2–3), 117 (2014).
[4]Y. Ogo, H. Hiramatsu, K. Nomura, H. Yanagi, T. Kamiya, M. Kimura, M. Hirano, and H. Hosono, Phys. Status Solidi A **206**(9), 2187 (2009).
[5]H. Shimotani, H. Suzuki, K. Ueno, M. Kawasaki, and Y. Iwasa, Appl. Phys. Lett. **92**(24), 242107 (2008).
[6]E. Fortunato, R. Barros, P. Barquinha, V. Figueiredo, S.-H. K. Park, C.-S. Hwang, and R. Martins, Appl. Phys. Lett. **97**(5), 052105 (2010).
[7]H. Yabuta, N. Kaji, R. Hayashi, H. Kumomi, K. Nomura, T. Kamiya, M. Hirano, and H. Hosono, Appl. Phys. Lett. **97**(7), 072111 (2010).
[8]J. A. Caraveo-Frescas, P. K. Nayak, H. A. Al-Jawhari, D. B. Granato, U. Schwingenschlögl, and H. N. Alshareef, ACS Nano **7**(6), 5160 (2013).
[9]Y.-J. Han, Y.-J. Choi, C.-Y. Jeong, D. Lee, S.-H. Song, and H.-I. Kwon, IEEE Electron Device Lett. **36**(5), 466 (2015).
[10]Y.-J. Han, Y.-J. Choi, I.-T. Cho, S. H. Jin, J.-H. Lee, and H.-I. Kwon, IEEE Electron Device Lett. **35**(12), 1260 (2014).
[11]H. Luo, L. Liang, H. Cao, M. Dai, Y. Lu, and M. Wang, ACS Appl. Mater. Interfaces **7**(31), 17023 (2015).
[12]T. Kamiya and H. Hosono, NPG Asia Mater. **2**, 15 (2010).
[13]M. D. H. Chowdhury, P. Migliorato, and J. Jang, Appl. Phys. Lett. **103**(15), 152103 (2013).
[14]D. Adler, L. P. Flora, and S. D. Senturia, Solid State Commun. **12**(1), 9 (1973).
[15]T. Kamiya, K. Nomura, and H. Hosono, J. Disp. Technol. **5**(12), 462 (2009).
[16]N. F. Mott, J. Non-Cryst. Solids **1**(1), 1 (1968).
[17]Y.-L. Huang, S.-P. Chiu, Z.-X. Zhu, Z.-Q. Li, and J.-J. Lin, J. Appl. Phys. **107**(6), 063715 (2010).
[18]S. Lee and A. Nathan, Appl. Phys. Lett. **101**(11), 113502 (2012).
[19]C.-Y. Jeong, D. Lee, Y.-J. Han, Y.-J. Choi, and H.-I. Kwon, Semicond. Sci. Technol. **30**(8), 085004 (2015).
[20]T. Kazushige, N. Mitsuru, E. Toshimasa, Y. Hirotaka, and K. Setsuo, Jpn. J. Appl. Phys., Part 1 **48**(7R), 078001 (2009).
[21]C. A. Dimitriadis, N. A. Economou, and P. A. Coxon, Appl. Phys. Lett. **59**(2), 172–174 (1991).
[22]W. E. Spear and P. G. Le Comber, Solid State Commun. **17**(9), 1193–1196 (1975).
[23]K. Nomura, T. Kamiya, and H. Hosono, Adv. Mater. **23**(30), 3431 (2011).
[24]S. Y. Lee, D. H. Kim, E. Chong, Y. W. Jeon, and D. H. Kim, Appl. Phys. Lett. **98**(12), 122105 (2011).
[25]A. Togo, F. Oba, I. Tanaka, and K. Tatsumi, Phys. Rev. B **74**(19), 195128 (2006).